been confirmed to be 30–40 ps by measurements of the relaxation oscillations in a long external cavity.

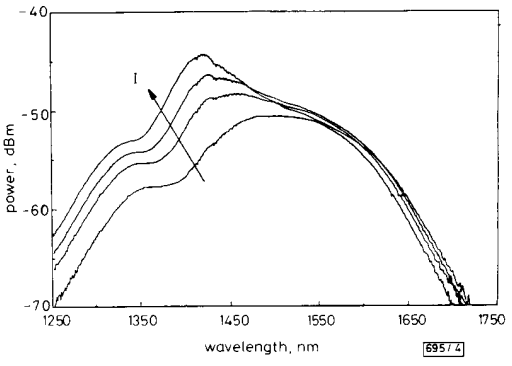

Fig. 4 *Spontaneous spectra against current*

The spontaneous spectrum response to a strongly saturating input signal in these MQW devices is different from that observed in bulk devices. In bulk devices the gain is depressed at all energies when a strongly saturating signal is present. The gain spectrum under saturation conditions is identical to the unsaturated spectrum at a lower injection current.[8] In these MQW devices, the carriers are preferentially used from energies higher than that corresponding to the input signal wavelength. At lower energies, the distribution of recombining carriers is virtually unaffected. This difference could be important in understanding the carrier dynamics underlying the gain recovery process in MQW as opposed to bulk amplifiers.

Conclusions: Saturated output powers of 115 mW at 3 dB gain compression have been obtained in GRIN-SC-MQW BH semiconductor laser amplifiers. Unsaturated gain of 8·4 dB improved with cavity length to 13·3 dB, but better AR coatings were required. Weak current dependence of gain near 1·5 μm was a result of the specific band filling found in quantum wells. In the saturated regime, carriers at energies higher than the signal's were preferentially used, in contrast to bulk devices where the gain is homogeneously depressed. This feature may underlie very fast gain recovery times.

Acknowledgment: The authors are grateful to P. E. Barnsley and Dr. D. M. Spirit for the use of the data in Fig. 3 and to I. W. Marshall for the relaxation oscillation measurements.

M. BAGLEY
G. SHERLOCK
D. M. COOPER
L. D. WESTBROOK
D. J. ELTON
H. J. WICKES
P. C. SPURDENS
W. J. DEVLIN

British Telecom Research Laboratories
Martlesham Heath, Ipswich, United Kingdom

1st February 1990

References

1 SIMON, J. C., LANDOUSIES, B., BOSSIS, Y., DOUSSIERE, P., FERNIER, B., and PADIOLEAU, C.: 'Gain, polarisation sensitivity and saturation power of 1·5 μm near-travelling-wave semiconductor laser amplifier', *Electron. Lett.*, 1987, **23**, pp. 332–334
2 SAITOH, T., and MUKAI, T.: '1·5 μm GaInAsP travelling-wave semiconductor laser amplifier', *IEEE J. Quant. Electron.*, 1987, **QE-23**, pp. 1010–1020
3 DEVLIN, W. J., *et al.*: 'Polarization insensitive high output power 1·3 and 1·5 μm optical amplifiers made by MOVPE'. Proc. IOOC 1989, Kobe, Japan, Paper ThC2
4 EISENSTEIN, G., *et al.*: '1·5 μm multiple quantum well optical amplifier with high saturated output power'. *Ibid.*, Paper 20PDB-13
5 COOPER, D. M., SELTZER, C. P., AYLETT, M., ELTON, D. J., HARLOW, M., WICKES, H., and MURRELL, D. L.: 'High power, 1·5 μm all-MOVPE buried heterostructure, graded index separate confinement multiple quantum well lasers', *Electron. Lett.*, 1989, **25**, pp. 1635–1637
6 NELSON, A. W., DEVLIN, W. J., HOBBS, R. E., LENTON, C. G. D., and WONG, S.: 'High power, low threshold BH lasers grown entirely by MOVPE', *ibid.*, 1985, **21**, pp. 888–889
7 BAGLEY, M., *et al.*: '242 nm continuous tuning from a GRIN-SC-MQW BH InGaAsP laser in an extended cavity', submitted to *Electron. Lett.*
8 INOUE, K., MUKAI, T., and SAITOH, T.: 'Gain saturation dependence on signal wavelength in a travelling-wave semiconductor laser amplifier', *Electron. Lett.*, 1987, **23**, pp. 328–329

OPTICAL FIBRE MICROBENDING SENSORS BY MICROMACHINING TECHNIQUES

Indexing terms: Optical fibres, Measurement

A practical tactile sensor using micromachined techniques has been implemented and evaluated. Optical fibres laid on the pedestals of micromachined silicon showed outstanding improvement in sensitivity, mechanical decoupling between fibres and excellent repeatability. The upper cover made from plastic and Cu–Be foils, not only provides a protective membrane to the sensor but also acts as the force concentrator, allowing better force point resolution.

Tactile sensors, showing touch characteristics of a human-like finger, are required in enhancing grippers and manipulators placed on the palm of a robotic arm. They are required for two major reasons. It is desirable to make sensors as small and light as possible maintaining a simple but high degree of force resolution. They are also required to measure the total force applied to objects being held by the gripper so as not to drop or crush them during manipulation. It is often required that the gripper sense an edge or flat surface before picking up the object. The resolution and position of the force is thus important in the use of a tactile sensor.

Light intensity modulation, induced by microbending loss in multimode fibres, can be utilised for detecting force and displacement. Light propagating in the optical fibres is immune to the ambient electrical and magnetic interference in a typical factor so optical sensors have many advantages over other types of sensor. Attenuation of light caused by microbending of the optical fibre is enhanced by imposing periodic perturbations. The force is then directly related to the light loss caused by the microbending. According to the mode coupling theory, the periodic perturbation function after Fourier transformation, has a coupling coefficient[1]

$$K_{AB}(z) = \sum_n K_n e^{-jn\beta z} \tag{1}$$

where $\beta = (2\pi/\lambda)$ and λ is the mechanical wavelength of the periodic perturbation. The coupled-mode equations for power coupling from mode A to mode B can be written as

$$\frac{da_B}{dz} = -j \sum_n K_n e^{-j(k-k'+n\beta z)a_A} \tag{2}$$

where $a_{A,B}$ is the amplitude of the field in mode A or B. To obtain the phase matching for optimum light power coupled between modes, the longitudinal propagation constant k and k' must satisfy[2,3]

$$k - k' = \pm\frac{2\pi}{\lambda} \tag{3}$$

Using the parabolic refractive index profile and applying the WKB approximation to the solution of the wave number separation of neighbouring modes, the important mechanical periodicity λ is given by[4]

$$\lambda = \frac{2\pi a n_0}{NA} \tag{4}$$

where n_0 is the refractive index of the core, a is the radius of the core, and NA is the numerical aperture of the fibre which can be expressed as

$$NA = \sqrt{(n_0^2 - n_{cladding}^2)} \quad (5)$$

For the fibres we used in this work, λ is 1·225 mm. Microbending light attenuation considered as coupling of guided to radiated modes for optical waves propagating in the optical fibres, can be greatly enhanced with the periodicity expressed in eqn. 3.

Current commercial fibre optic sensors have encountered two problems. One problem is how to accurately fabricate the critical periodic length of the deformation object so that the microbend effect can be increased through the correct corrugation periodicity. The other problem is how to overcome the erroneous data received from the fibres surrounding the actually active pixel caused by the mechanical coupling and the repeatability of force response along with the hysteresis problems caused by fibre slippage and bowing during evaluations.

Micromachined silicon wafers have already been used for fibre-guiding grooves, laser-to-fibre couplers and channel waveguides.[5] This letter describes a practical micromachining method for silicon wafers, a novel cover with a compliant membrane on top of the wafer, and a unique array of pedestals with only two layers of optical fibres that allows full force resolution. The whole sandwich like design is capable of solving several of the problems mentioned previously.

The micromachined techniques reported here use the growth of an isolation layer on silicon wafers, photolithography, and anisotropic wet etching. The anisotropic etching solution for the Si wafer is a mixture of weight with 23·4% potassium hydroxide (KOH), 63·3% DI water and 13·3% N-propanol used at 81°C with a gentle agitation. Ethylenediamine (ED), pyrocatechol (P) and water could have been used for the etch (EDP) with similar results.[6] The fabrication process for the grooves and mesas is illustrated in Fig. 1*a* using standard integrated circuit techniques. The thermally grown SiO_2 layer serves as the isolation layer against wet etching which produced the mesa height of about 64 μm. The depth of the small groove is around 20 μm as shown in Fig. 1*b*.

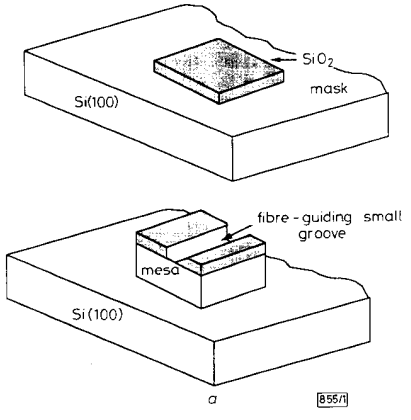

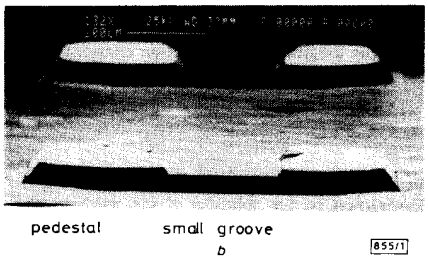

Fig. 1 *Silicon mesas and grooves*
a Fabrication process
b Micrograph

The unique pedestal array is a face-centred cubic (FCC) with small etched grooves on top of the mesas. The reason for the small grooves is to fix the fibres from bowing sideways and for easy assembly. Fig. 2 illustrates the bottom layer of fibre placed in the grooves. A second layer of fibres are then placed orthogonal to the bottom layer and aligned to the pedestal array.

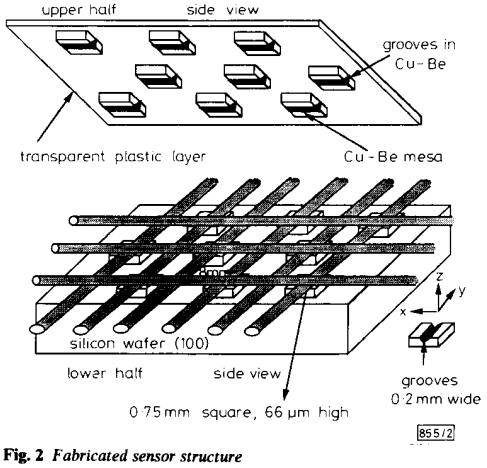

Fig. 2 *Fabricated sensor structure*

The compliant Cu–Be membrane was fabricated with the same photolithography mask and procedure but with a different etching solution containing 55·2 gm of $FeCl_3$ and 99 ml of H_2O. The Cu–Be foil is first glued to the thin plastic layer. This layer is transparent so the Cu–Be posts can be properly aligned to the FCC bottom array. The isolation layer against the $FeCl_3$ solution is photoresist. The Cu–Be layeer after etching has been completely lifted out leaving only those mesas with the same height as the original thickness of the Cu–Be sheet (3 mil = 73·5 μm). The mesas on the cover are then positioned at the offset points of the silicon wafer, off by one half a lattice constant. The spacing between each mesa was 2 mm. Fig. 2 shows the whole structure and the layout of the fibres. The transparent layer on the cover provides clear vision during the evaluation steps and a smooth force surface that protects the sensor. Micromachined grooves on the membrane layer of mesas hold the fibres in the x-direction while on the silicon pedestals fix the fibres in the y-direction. For assembly, the x-direction fibres are fixed by the grooves on the Cu–Be cover. Each fibre is connected to an LED diode at one end and to a PIN diode at the other end. Finally fibres are placed under tension and cemented at the edge of the silicon wafer with epoxy glue.

The optical fibre sensor was tested unsing a calibrated force which exerts a known amount of force to specific pixels or group of pixels. The input and output intensity are both monitored by a personal computer and force as a function of attenuation is recorded. The repeatability and mechanical de-coupling effects between fibre are shown in the plots of Fig. 3, where the fibres are labelled as shown in left hand side of the Figure. Only the fibres crossing at the active pixel show attenuation. Hence the large degree of mechanical de-coupling between fibres on both levels, an improvement of 19 dB over previous designs.[7] As a result the location and amount of actual force can be determined. The splitting of the two response curves C1 and L11 is caused by the tension imposed on different layers of fibres and because the top layer is at a different height from the sensor bottom. Adjusting the initial tension reduces the split between the fibres response.

Fig. 3 also shows the mean values and standard deviation values for ten repeated runs. Since the fibres are fixed by the grooves, the repeatability response is greatly improved when compared with previous work.[7] Hysteresis is generally caused

by two factors; the fero-fluid in the actuator's magnetic gap and sensor drift caused by fibres slipping or bowing. The second factor has almost been eliminated and the hysteresis value has been reduced to 0·014 NT because of the grooves.

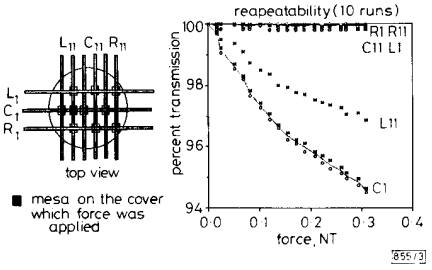

Fig. 3 *Repeatability response of sensor*

The sensitivity of a microbending sensor is essentially dependent on four factors. The size of the deformation amplitude, the proximity to the critical deformation periodicity when the pedestal array is fabricated, the number of microbends, and the length of the sensing fibres, all affect the sensitivity of the sensor. Each sensor design has its own limitations. The tactile sensor presented here is limited by the heights of the mesas which can only provide 40 μm deformation amplitude. Compared to the same type of sensor, the sensitivity has been increased by 8·5 dB. Precise micromachining techniques, with an accuracy of within 0·1%, can enhance the resolution range.

In conclusion, a micromachined optical fibre sensor has been demonstrated. A face-centred cubic mesa structure with grooves on top successfully eliminated the mechanical coupling between fibres. The guiding grooves for the optical fibres increase the repeatability of the sensor response and reduce the hysteresis effect. The microbend effect through the correct corrugation periodicity has also been greatly improved.

The authors wish to thank Dr. C. L. Chen and Mr. S. R. Emge for providing their testing instruments and for technical assistance, and Ms. Fei Luo for her work on the cover fabrication. This work was supported by the National Science Foundation under Grant CDR 8803017 to the Engineering Research Center for Intelligent Manufacturing Systems.

J. H. C. CHAO
G. W. NEUDECK
School of Electrical Engineering
Purdue University
West Lafayette, Indiana 47907, USA

26th February 1990

References

1 LEE, D.: 'Electromagnetic principles of integrated optics' (John Wiley and Sons, New York, 1986)
2 KECK, D. B., and BARNOSKI, M. (Ed.): 'Fundamentals of optical fiber communications' (Academic, New York, 1976)
3 WIDWINTER, J. E.: 'Optical fibers for transmission' (Wiley, New York, 1979)
4 LAGAKOS, N., COLE, J. H., and BUCARO, J. A.: 'Microbend fiber-optic sensor', *Appl. Opt.*, 1986, **26**, (11), pp. 2171–2180
5 YAMADA, Y., KAWACHI, M., and KOBAYASHI, M.: 'Optical-fibre coupling to high-silica channel waveguides with fiber-guiding grooves', *Electron. Lett.*, 1984, **20**, pp. 313–314
6 BASSOUS, E.: 'Fabrication of novel three-dimensional microstructures by the anisotropic etching of (100) and (110) silicon', *IEEE Trans.*, 1978, **ED-10**, (10), pp. 1178–1185
7 JENSTROM, D. T., and CHEN, C.-L.: 'A fiber optic microbend tactile sensor array', to be published in *Sensors and Actuators*

ULTRA-HIGH GAIN, LOW NOISE MONOLITHIC InP HEMT DISTRIBUTED AMPLIFIER FROM 5 TO 40 GHz

Indexing terms: Semiconductor devices and materials, Amplifiers, Indium compounds

A monolithic 5–45 GHz distributed amplifier has been developed utilising 0·25 μm InAlAs/InGaAs lattice matched HEMTs with a mushroom gate profile as active devices. A measured gain of 12·5 $\pm$ 0·5 dB from 5 to 40 GHz and a measured noise figure of 2·5–4 dB in the Ka-band were achieved.

Introduction: Monolithic distributed amplifiers using conventional AlGaAs/GaAs HEMTs or AlGaAs/InGaAs pseudomorphic HEMTs as active devices have been reported with frequencies up to 70 GHz.[1,2]

InAlAs/InGaAs HEMTs lattice matched to InP have demonstrated higher gain and lower noise figure compared with AlGaAs/GaAs and AlGaAs/InGaAs pseudomorphic HEMTs. A monolithic microstrip-type distributed amplifier utilising InP HEMTs as the active devices was reported with an 8 dB gain from 2 to 35 GHz.[3] A 5–100 GHz InP coplanar waveguide MMIC distributed amplifier with an average gain of 5 dB has recently been reported.[4]

This letter describes the results of a 5–40 GHz monolithic microstrip-type distributed amplifier using 0·25 μm InP HEMTs having a mushroom gate profile as the active devices. An ultra-high gain of 12·5 dB from 5 to beyond 40 GHz and a noise figure of 2·5–4 dB in the Ka-band were measured. These are the best results reported to date.

Device considerations: Fig. 1 shows the InAlAs/InGaAs lattice matched HEMT epitaxial growth structure used in the amplifier. A discrete 0·25 × 150 μm HEMT has a typical extrinsic g_m of 800 mS/mm, an intrinsic g_m of 1200 mS/mm, a pinch-off voltage of 0·6 V and a breakdown voltage of 3 V. This device has a measured MAG of 12 dB at 40 GHz, an extrapolated f_t of 90 GHz and an f_{max} of 200 GHz.

Circuit design: A distributed amplifier consisting of five 0·25 μm HEMTs with variable gate widths and on-chip biasing circuits was designed with a cutoff off frequency of 45 GHz. The total gate width is 350 μm. Fig. 2 shows the SEM photograph for the distributed amplifier. The chip size is 2·3 × 0·9 mm.

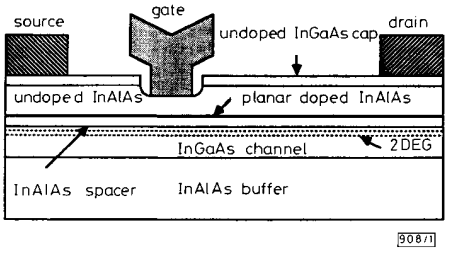

Fig. 1 *Cross-section of InP HEMT*

MMIC fabrication: Standard MMIC processing techniques were used for the monolithic InP HEMT distributed amplifier fabrication. The two critical process steps involved are the 0·25 μm E-beam gate with a mushroom gate profile and the 60 × 60 μm backside vias using a recently developed novel wet etch process.

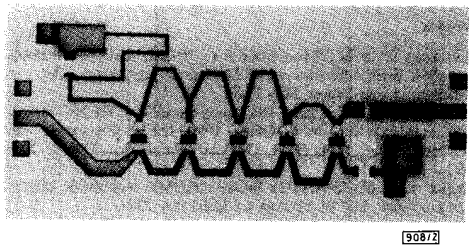

Fig. 2 *5–45 GHz monolithic InP HEMT distributed amplifier*